Geosci. Model Dev., 19, 11019–11039, 2026
https://doi.org/10.5194/gmd-19-11019-2026
© Author(s) 2026. This work is distributed under
the Creative Commons Attribution 4.0 License.

Geoscientific Model Development
Open Access
EGU

Implementation of the reduced complexity model InMAP at urban scale using a high-resolution WRF-Chem simulation

Diego Roberto Rojas Neisa, Alejandro Piracoca-Mayorga, Sebastián Espitia-Cano, Ivan Romero-Martinez, and Ricardo Morales Betancourt

Department of Civil and Environmental Engineering, Universidad de los Andes, Cra. 1A 18-5, Bogota, Colombia

Correspondence: Ricardo Morales Betancourt (r.moralesb@uniandes.edu.co)

Received: 21 February 2026 – Discussion started: 6 March 2026
Revised: 8 November 2026 – Accepted: 9 November 2026 – Published: 19 November 2026

Abstract. Most of the population globally lives in areas exceeding prior and current WHO guidelines for fine particulate matter ($PM_{2.5}$), highlighting the persisting need for implementing emission reduction strategies. Given the complex transport and transformation processes that airborne species undergo in the atmosphere, chemical transport models can aid in designing and prioritizing air pollution mitigation actions. However, detailed chemical transport models often require substantial computational power and expertise. For that reason, reduced complexity models have emerged as an alternative, incorporating some of the information from chemical transport models while drastically reducing the technical complexity and computational demand. In this work, we build a local implementation of the Intervention Model For Air Pollution, InMAP, at high spatial resolution for a large urban area, in Bogotá, Colombia. As input for the reduced complexity model, we carried out a detailed 12-month simulation with the Weather Research and Forecasting model coupled with Chemistry (WRF-Chem) version 3.9.1. To achieve sufficiently high spatial-resolution for urban air quality, the model was configured with three nested domains of 27×27 9×9, and 3×3 km respectively. When compared with surface station data, the modeled annual mean $PM_{2.5}$ showed a slight $+2.7\,\%$ overestimation at the city-scale. Furthermore, the WRF-Chem simulation captured the structure of the observed $PM_{2.5}$ time series at daily, weekly and seasonal timescales. The InMAP base fields showed a moderate underprediction relative to WRF-Chem, but overall, the Pearson correlation between the WRF-Chem and InMAP modeled $PM_{2.5}$ fields was $r = 0.91$. InMAP sensitivity was tested for three emission reduction scenarios of varying complexity, by comparing the marginal concentrations against simulations with the full chemical transport model. The scenarios ranged in complexity, from primary-PM reductions only, to scenarios exploring moderate and severe city-wide emissions reductions from diesel powered mobile sources. Although InMAP marginal $PM_{2.5}$ fields were linearly correlated with the corresponding WRF-Chem sensitivities, a strong overestimation in predicted $PM_{2.5}$ variations were shown for all emission reduction scenarios considered. For the simpler scenarios where only primary PM was reduced, the ratio of InMAP to WRF-Chem sensitivity was a factor of 2.0 (C.I. 1.81–2.35), while for the more complex emission reduction scenarios involving also reduction in gas-phase emissions, the same ratio of sensitivities was a factor of 5.0 (C.I. 4.22–5.79). The large sensitivity shown by InMAP in the scenarios involving gas-phase precursors is a large overestimation of secondary organic aerosols and particulate nitrate. The results of this work suggest that InMAP can be used to scan for potential emission reduction scenarios at the urban-scale, specially when those scenarios involve mostly primary PM emission reductions. However, our analysis indicates that studies aiming to carry out assessments using the absolute reductions in concentration from InMAP should use the results with caution, as the uncertainties might be large.

1 Introduction

Exposure to air pollutants, especially to fine particulate matter ($PM_{2.5}$), negatively impacts human health, with estimates indicating several million excess deaths globally are attributable every year to poor air quality (e.g., Burnett et al., 2018). Both, chronic and episodic exposure to PM is asso-

ciated with increased mortality (e.g., Chen and Hoek, 2020; Orellano et al., 2020). Multiple emission sectors contribute to the $PM_{2.5}$ concentration, with the relevance of different sources varying regionally (McDuffie et al., 2021). Despite the progress that has been achieved in some regions of the world in reducing particulate pollution, most of the population globally, specially in low- and middle-income countries, still experience fine particulate concentration at levels much higher than the WHO guidelines (Brauer et al., 2016). Therefore, continued efforts to reduce atmospheric emissions are necessary to reduce the negative health burden of air pollution.

Given the complex atmospheric chemistry and transport processes that determine the level of air pollution at any given location, emission reductions in a specific site or sector might have varying degrees of impact over air pollutants concentrations elsewhere. Therefore, sensible emission reduction policies must consider not only primary emissions, but how atmospheric transport and transformation dictate its air pollution impact. The tool most suited to address the interactions resulting from atmospheric processes are comprehensive chemical transport models, or CTMs. These state-of-the-science models, which involve mechanistically resolving atmospheric transport, gas-phase chemistry, aerosol transformations, and other processes have undergone continuous development over more than two decades. Multiple comprehensive CTMs are currently available, some of the most widely used include CAM-Chem (Emmons et al., 2020), CMAQ (Appel et al., 2017), CHIMERE (Menut et al., 2024), and WRF-Chem (Grell et al., 2005). Involving CTMs in the design of air pollution reduction strategies, although complex, can lead to science-based policies, likely enhancing the effectiveness of such policy if implemented. However, the high requirement for computational resources intrinsic to running CTMs and the expertise needed to set-up and execute such models are not always available to air quality managers and decision makers. To offset these limitations, simpler models, often termed reduced-complexity models (RCM) or reduced-form models, have been developed (e.g., Tessum et al., 2017; Heo et al., 2016b; Thunis et al., 2016).

Among the key characteristics of reduced-complexity models is the drastic reduction in computing time and simpler input data structure requirements compared to those of a CTM. These characteristics make RCM suitable for quickly scanning multiple emission reduction scenarios and to analyze their potential impact on air pollution. Multiple approaches have been used over the years to overcome the high-computational burden of CTMs while still producing scientifically- or policy-relevant results. The EASIUR model (Heo et al., 2016b) uses an statistical approach on the output of multiple CTM runs (spatial resolution 36 km × 36 km) to efficiently derive marginal benefits from emission changes. Other RCMs, such as APEEP (e.g, Muller and Mendelsohn, 2009) are derived from repeated application of simpler Gaussian dispersion models. EASIUR and APEEP have been applied mostly to estimate social costs of air pollution emissions at the county level in the US (Muller and Mendelsohn, 2009; Heo et al., 2016a; Gentry et al., 2023, e.g.,). Other RCMs have used variants of the statistical approach. The SHERPA tool (Thunis et al., 2016, 2018) uses multiple CTM model runs to develop linear source-receptor matrices (Clappier et al., 2015). Trained on outputs from the European CHIMERE model (Menut et al., 2024), this tool has been extensively used to estimate air pollution attributable mortality in European cities (Khomenko et al., 2023). Other RCMs, such as the Intervention Model For Air Pollution, InMAP, (Tessum et al., 2017) have departed from the statistical approach in favor of a more physically-based estimate of annual mean marginal concentration changes. The methodology used in InMAP is based on solving a steady-state version of the continuity equation for certain chemical species considering physical and chemical processes including advection, turbulent mixing, atmospheric aerosol chemistry, dry deposition, and wet deposition (Tessum et al., 2017). As most other RCM, InMAP requires several orders of magnitude less computational resources compared to those of a full CTM (e.g., Goodkind et al., 2019). Yet, the main input necessary to build a version of InMAP consist of three-dimensional time-varying meteorological and air pollution fields produced from a CTM for the specific modeling domain.

InMAP has been utilized to determine source-receptor matrices in the continental United States, referred to as InMAP-US (Goodkind et al., 2019), by informing the model with a 12 km spatial resolution WRF-Chem simulation (Tessum et al., 2015). RCMs are often employed for scenario analysis. In the US, several RCMs, including InMAP-US, have been used to analyze the potential impact of widespread adoption of electric vehicles (e.g., Choma et al., 2020; Gentry et al., 2023). InMAP has also been implemented over China (InMAP-China) using the WRF-CMAQ CTM at a 36 km spatial resolution (Wu et al., 2021). Furthermore, a global implementation of InMAP (Global-InMAP) is currently available (Thakrar et al., 2022). For that implementation, the CTM information was provided by the global model GEOS-Chem, with a resolution of $2° \times 2.5°$. Although valuable to understand large-scale impacts of emission reductions, such coarse spatial resolution is of little use when addressing local emission sources or regions where concentration gradients are large, due to spatial heterogeneity in emissions, topography, or population density, like those often found in compact urban areas. Despite those limitations, Global InMAP has been used to explore the contribution of external sources in large urban centers globally (Tessum et al., 2022). The spatial resolution of global CTMs is likely not sufficient to resolve intra-city air pollution gradients, and it is also likely that the emissions used in global CTMs often lack local emission data for many cities worldwide.

However, there has not been widespread implementations of RCMs in the global south, and, to our knowledge, none in

Latin America, which are precisely those regions were availability of state-of-the-science CTMs is scarcer and where emissions data might be missing. In the case of Colombia, the development of detailed urban-scale emission inventories(Pachón et al., 2018) has facilitated the application of state-of-the-art CTM models to study regional and urban air quality. Among the models that have been implemented are CMAQ, driven by WRF meteorology, which was used to explore urban-scale emission reduction scenarios (e.g., East et al., 2021). The WRF-Chem model has been used to estimate the contribution of regional biomass burning sources to air pollution in the city of Bogotá (Ballesteros-González et al., 2020, 2022). However, such studies have been limited to short simulations periods and have not been systematically used to inform urban-scale prioritization of emission reductions.

In this work, we partially address the lack of RCM applications in Latin America and the coarse resolution of other studies, unsuitable for urban-scale analysis, by implementing and evaluating InMAP for the city of Bogotá in Colombia (InMAP-BOG), a large urban area in the global south. For this, we extended existing CTM capabilities developed in previous studies (e.g., Ballesteros-González et al., 2020, 2022) and extend them to a full-year simulation at resolutions relevant for urban-scale air pollution analysis. Because long-term exposure to particulate matter has shown to have the strongest association with health outcomes, we focused on the annual average variations in $PM_{2.5}$ concentration resulting from marginal emission changes relative to a baseline scenario.

To our knowledge, this is one of the first local implementations of InMAP outside of China and the United States, and the only using high-resolution emission data and parameterized with a comparable-scale full CTM simulation. Some research is being conducted to implement InMAP for India (Balasubramanian et al., 2026). We built InMAP locally by carrying out a detailed high-resolution (3×3 km) 12-month simulation with the WRF-Chem chemical transport model as input for the reduced complexity model. Besides evaluating the model-to-model base case simulation, we also carried out sensitivity tests with the full CTM and tested the same scenarios with InMAP-Bog. With this work we aim to explore the ability of InMAP to scan high-resolution emission abatement policies and to inform air quality management options. We explore the benefits in exposure from cell-by-cell reductions in emissions. We also discuss the possible future applications of this model for policy use, its limitations, and potential strategies to overcome those limitations.

2 Methods

The methodology in this study involved three steps. The first, was completing a 1-year simulation with a chemical transport model at a resolution relevant for resolving intra-urban gradients in air quality, and then assessing its skill to reproduce ground-based air pollution datasets. The second was to use the outcome of that detailed CTM simulation to build InMAP-Bog and to test its sensitivity against that of the full CTM simulation. The third step was to utilize InMAP to quickly scan spatially-resolved emission reduction scenarios for policy use.

2.1 Implementation of InMAP

Typically, atmospheric models explicitly solve coupled mass conservation equations involving advection and turbulent transport as well as chemical transformations and removal from the atmosphere through deposition. In InMAP approach, gas-phase and particulate pollutant concentrations are computed through an approximate steady-state solution to the continuity equation for a given species

$$\frac{\partial c_i}{\partial t} = \nabla \cdot (K \nabla c_i) - \nabla \cdot (\overline{\boldsymbol{v}} c_i) + r_i + E_i - d_i \quad (1)$$

where, c_i is the concentration of species "i", whose tendency, $\partial c_i / \partial t$, is determined by advection by the mean wind vector ($\bar{\boldsymbol{v}}$) as well as by turbulent atmospheric transport, quantified here by the turbulent mixing parameter K. Additionally, any given species can be produced or consumed by multiple chemical reactions, which are represented by the net formation rate of species r_i, and can be removed by wet and dry deposition to the surface (d_i). In Eq. (1) E_i is the emission rate of the species i, which can be from anthropogenic and natural sources. In its simplified approach, InMAP produces only annual average pollutant concentration fields. The chemical species considered by InMAP are primary $PM_{2.5}$, volatile organic compounds (VOCs), secondary organic aerosol (SOA), sulfur dioxide (SO_x), particulate sulfate (pSO_4), oxides of nitrogen (NO_x), particulate nitrate (pNO_3), ammonia (NH_3), and particulate ammonium (pNH_4). InMAP must be compiled by providing it with hourly outputs from a one-year simulation with a full CTM, which are used by InMAP steady-state solution algorithm to extract atmospheric properties necessary to infer annual mean concentration fields. For advection and turbulent mixing at the lateral boundaries of the domain InMAP uses a zero concentration-change approach (Tessum et al., 2017). The lateral inflow of species, which is explicitly treated by the driving CTM, is key to determine the concentration levels for the baseline scenario. However, since the model objective is to solve a steady-state equation for the difference in concentrations caused by localized policy interventions or emission shifts, the approach used by InMAP is justified . For a full description of InMAP the reader is referred elsewhere (e.g., Tessum et al., 2017), but we provide here the key variables linking it with the driving CTM simulation. In its original implementation, InMAP was driven by WRF-Chem v3.4 as the CTM providing the detailed fields (Tessum et al., 2017), with a domain covering North America at a resolution of 12 km. In this work

we used a different version of the same CTM, WRF-Chem version 3.9.1, to provide the detailed simulation needed by InMAP, and therefore closely followed the original InMAP implementation as described in that work. From the three-dimensional WRF-Chem hourly output fields, which were organized in daily files, the necessary input variables were extracted and provided to InMAP. The complete list of WRF-Chem variables used by the InMAP preprocessor and how they are used is reported in Table E1, which is reproduced from the description of InMAP-US (see Table S1 in Tessum et al., 2017). In contrast to other implementations of InMAP, we used higher spatial resolution (3 km × 3 km) and used a locally developed anthropogenic emission inventory. Given the modeling domain location at the equator, the WRF-Chem simulation was carried out using a Mercator projection. However, the default InMAP version 1.9.6 code, which was used in this work, only supports input data in either Lambert conformal projection (appropriate for mid-latitude domains) or in latitude-longitude format (used for global domains). To overcome this limitation, we included this capability through a minor source code modification, ensuring the correct processing of the Mercator projected input data. Our analysis is focused on a specially understudied region in terms of atmospheric chemical transport modeling. The details of the modeling domain and the WRF-Chem configuration are provided below.

2.1.1 Modeling domain

The relevant domain in this study is a 207 × 207 km region in central Colombia, with approximately 12.8 million people residing within the domain. The modeling was carried out with a horizontal resolution of 3 km × 3 km centered in the city of Bogotá (Fig. A1). With its population estimated at 8 million, the city is one of the most densely populated in Latin America (Wheeler, 2015), and is located 2600 m a.s.l. (above sea level) in the equatorial Andean region of South America. The urban buildup is compact, spanning only 380 km^2, and therefore, the gradient between dense-urban and rural land-use is sharp. Additionally, the topography surrounding the city is complex, with nearby mountains reaching up to 4000 m (Fig. 3). According to the local air quality monitoring network, annual mean $PM_{2.5}$ was 17.2 $\mu g\, m^{-3}$ in 2018, exceeding the World Health Organization (WHO) guidelines (WHO, 2021). Furthermore, largely due to regional biomass burning emission and large-scale meteorological conditions, the city experiences significant seasonal variation in $PM_{2.5}$ and other air pollutants, with two annual concentrations peaks, the first between January to March, and the other in September and October (Mendez-Espinosa et al., 2019). The 24 h $PM_{2.5}$ routinely exceeds the daily local limit of 37 $\mu g\, m^{-3}$, and consequently, exceeds many times over the WHO air quality guidelines for 24 h exposures. Most of those exceedances occur in the south-west of the city were industrial sources and heavy duty traffic are prevalent (East et al., 2021). Concentrations are much lower from June to September.

Table 1. WRF-Chem model parameterization.

Parameter	Scheme	Reference
Microphysics	Lin et al.	Lin et al. (1983)
Longwave Radiation	RRTM	Mlawer et al. (1997)
Shortwave Radiation	Dudhia	Dudhia (1989)
Land Surface	Noah	Ek et al. (2003)
Planetary Boundary Layer	YSU	Hong et al. (2006)
Cumulus	Grell-Freitas	Grell and Freitas (2014)
Gas-phase Chemistry	RACM	Stockwell et al. (1997)
Aerosol Mechanism	MADE	Ackermann et al. (1998)
SOA Scheme	VBS	Ahmadov et al. (2012)

2.1.2 Base Simulation with WRF-Chem

We used the Weather Research and Forecasting model coupled with Chemistry (WRF-Chem) version 3.9.1, a meteorological and chemical transport model (e.g., Grell et al., 2005; Fast et al., 2006; Powers et al., 2017) as the driver for the RCM InMAP. The model configuration used in this study closely follows that of previous studies (e.g., Ballesteros-González et al., 2020, 2022), which have shown good skill in reproducing observed concentrations. However, those previous studies carried out simulations limited to just two months of the year as they were focused on quantifying regional biomass burning contributions to urban air quality. The main configuration parameters are summarized in Table 1. The selected aerosol scheme, particularly relevant given the focus of this study on $PM_{2.5}$, was the Modal Aerosol Dynamics model for Europe (MADE) (Ackermann et al., 1998) with a Secondary Organic Aerosol (SOA) formation mechanism based on the Volatility Basis Set approach (MADE-VBS) (Ahmadov et al., 2012). The MADE-VBS scheme uses 3 log-normal aerosol modes to describe the particles size distribution, including a nucleation, accumulation and coarse modes. The model accounts for SOA formation using the VBS approach, which groups organics species according to its volatility and uses partitioning theory to estimate a gas-phase and a particle-phase amount of organic species (Donahue et al., 2009), and couples it with the gas-phase chemistry scheme. RACM, the gas-phase chemistry mechanism, includes 78 chemical species and 214 gas-phase reactions (Stockwell et al., 1990, 1997).

Two minor bug-fixes were introduced in the WRF-Chem code. To prevent chemical species to erroneously reinitialize to low values on restart runs a simple flag was added in the corresponding aerosol module (*module_aerosol_soa_vbs.F*). In addition, when using the plume rise module with the MADE-VBS organic aerosol scheme, only the gas-phase species were being transported vertically by the plume rise. This was corrected by modifying the appropriate module

(*module_add_emiss_burn.F*). The source code for this modification is freely available (Rojas Neisa et al., 2026).

To achieve the sufficiently high spatial resolution necessary for urban air quality assessment in a compact city layout like the one in Bogota, WRF-Chem was configured with three nested modeling domains (Fig. A1). For this, the one-way nesting method was used, in which the larger domains provide the boundary and initial conditions for the inner domains. Initial and boundary conditions for the outermost domain were obtained from the global chemical transport model CAM-Chem (Emmons et al., 2020), $0.9° \times 1.25°$ (roughly 100 km × 125 km horizontal resolution) and 56 vertical levels, and mapped to the WRF-Chem domain boundaries. The three nested WRF-Chem simulations were used to downscale CAM-Chem fields to increasingly higher horizontal resolutions corresponding to 27×27 km (D01), 9×9 km (D02), and 3×3 km (D03) respectively. The model was configured with 41 eta-coordinate vertical levels, with 14 of those allocated to the lowest 1 km layer closest to the surface. This configuration has been used successfully in the past for shorter 2-month simulations exploring biomass burning impacts in the region (e.g., Ballesteros-González et al., 2020, 2022). However, in order to reduce the computational requirements and carry out longer simulations for the highest-resolution domain, a smaller D03 domain was specifically designed for this work. Instead of the 132×132 cells used in the D03 in Ballesteros-González et al. (2020), a smaller 69×69 cells domain, keeping the same horizontal and vertical resolution, was used in this study. This allowed to extend the simulation to a full year, and to explicitly explore emission reduction scenarios, while maintaining sufficient buffer grids at the domain boundaries. Since the study area is the city of Bogotá, we will focus exclusively on the highest-resolution domain. Details of the full modeling domain are included in Appendix A. The initial and boundary conditions for the meteorological fields were extracted from the National Center for Environmental Prediction Final Operation Global Analysis (NCEP-FNL) provided, which has a spatial resolution of 1° and 6-hourly temporal resolution (NCEP, 2000). Higher resolution runs at 1×1 km were attempted to further capture finer-scale details in the air pollution fields, but they were frequently interrupted by numerical instabilities, and could not be used in this work.

2.1.3 Emissions

For the urban perimeter of Bogotá we used detailed emissions from a locally-developed emission inventory for the year 2018 (Pachón et al., 2018). The Bogotá local emission inventory has a 1 km × 1 km resolution and includes emissions from commercial, mobile, and industrial sources. To accurately capture day-to-day variations in activity, we applied specific activity profiles for workdays, Saturdays, and Sundays or holidays. This was done for mobile, industrial and commercial sources. Similarly, to account for week-to-week activity changes and to capture seasonal changes in activity, the weekly ridership data from the public transport system was used as a proxy (Fig. B1). For PM, re-suspended particulate matter (RPM) sources are included, as those have been shown to be a significant source of primary PM in the city. For RPM emissions, we applied a monthly mitigation factor linked to precipitation, which modulates such emissions when the road surface is wet (Pérez-Peña et al., 2017).

Emissions outside of the urban perimeter, where no data from the local emission inventory is available, were extracted from the Emissions Database for Global Atmospheric Research version 4.3.1 (EDGAR V4.3.1) at $0.1° \times 0.1°$ horizontal resolution (Crippa et al., 2016). Given its relevance in the domain, we included biomass burning emissions from the Fire Inventory from NCAR, FINN version 1 (Wiedinmyer et al., 2011) for the three domains. FINN has hourly temporal resolution and spatial resolution of 1 km × 1 km. To correctly simulate the transport of biomass burning plumes emissions, which are injected at height, we used the 1-dimensional plume-rise model embedded into WRF-Chem (Grell et al., 2011). Although the innermost domain is located far from the main biomass burning sources in the region, previous modeling and observational studies (Rincón-Riveros et al., 2020) suggest its overall contribution to $PM_{2.5}$ is significant during some months. However, as those emissions are a regional-scale phenomena, they will not be affected by emission reduction strategies at the city-scale, which are the subject of analysis in the current work.

Biogenic emissions are calculated online using the Model of Emissions of Gases and Aerosols from Nature, MEGAN (Guenther et al., 2012), with emissions rates varying according to meteorological variables.

2.2 Scenario analysis with InMAP

To assess the skill of InMAP to predict changes in air pollution associated with diverse emission reduction scenarios, we set-up three hypothetical emission reduction scenarios in which emissions from one specific sector were decreased (Table 2). For those scenarios, we also conducted simulations with the full WRF-Chem model, so a direct comparison of the sensitivity of InMAP to emission reductions to those of the full CTM could be completed. The scenarios were built spanning diverse characteristics, considering emission sectors that are relevant for the city, but also considering the complexity in the type of emissions reduced in a given scenario. Similar scenarios had been previously analyzed but simulations had been carried out for just a couple of months (Bonilla et al., 2023). The scenarios range from primary PM only reductions (i.e., no gas phase emission reductions) to more complex settings involving the removal of emissions from diesel-powered mobile sources. The latter reduces all emission fluxes associated with the diesel power mobile sources, including gas-phase species, primary PM and gas-phase secondary aerosol precursors.

Table 2. Description of testing emission scenarios.

Scenario	Description
RPM-100	Resuspended dust emissions set to cero
Diesel-10	10 % reduction in diesel-powered mobile emissions
Diesel-100	100 % reduction in diesel-powered mobile emissions

3 Results

3.1 WRF-Chem simulation performance

The $PM_{2.5}$ concentration fields from the WRF-Chem simulation for the year 2018 showed close agreement with observations at different temporal scales. The modeled and observed timeseries of daily $PM_{2.5}$ for the city of Bogotá are shown in Fig. 1a. The WRF-Chem simulation accurately captures the structure of the time series, including the annual cycle of concentration with higher concentrations mainly in January-March and peaking again in October-November. Week-to-week variations seem to be captured accurately by the model. Those variations are largely likely explained by regional events, but some local variations in emissions linked to city dynamics can contribute to the observed changes. The observed and modeled annual mean $PM_{2.5}$ for the city were 17.26 and 17.72 $\mu g\,m^{-3}$, respectively, demonstrating a slight +2.7 % overestimation at the city-scale. Comparison of the standard deviation of daily concentration shows the model captured the variability of the $PM_{2.5}$ daily data. The standard deviation of modeled daily concentrations was 7.3 $\mu g\,m^{-3}$, in contrast to the observed standard deviation of 6.9 $\mu g\,m^{-3}$. At the daily scale, the Pearson correlation between the model and observed data is 0.64 (Fig. 1b).

Although the urban area of Bogotá is relatively compact, intra-urban patterns in $PM_{2.5}$ distribution were also well represented in the simulations, with the model capturing the observed northeast-to-southwest concentration gradient (Fig. 2). A statistical evaluation of the model performance in relation to established benchmarks for $PM_{2.5}$ (Emery et al., 2017) and meteorological variables (Emery et al., 2001) at individual air quality monitoring sites is shown in Appendix C. Overall, the results suggest the baseline WRF-Chem simulation is capable of reproducing the spatial and temporal variations in $PM_{2.5}$ at the urban scale in a way consistent with observations.

3.2 InMAP baseline

The comparison of InMAP and WRF-Chem predicted $PM_{2.5}$ fields for the base simulation are shown in Fig. 3. When analyzed over the entire D03 modeling domain, the mean $PM_{2.5}$ are 11.3 and 10.8 $\mu g\,m^{-3}$ for WRF-Chem and InMAP respectively, equivalent to a mean bias of $-0.50\,\mu g\,m^{-3}$, a RMSE of 1.07 $\mu g\,m^{-3}$, and a NMB −4.61 % implying InMAP base $PM_{2.5}$ is biased low but with small absolute and relative errors. The bias is not spatially homogeneous, with the South-eastern portion of the domain, which is geographically located in the eastern plains of the country, showing an overestimation of $PM_{2.5}$ relative to WRF-Chem. Over the rest of the domain InMAP underestimates $PM_{2.5}$ fields relative to the full CTM simulation. Previous studies suggest that over the eastern lowlands, $PM_{2.5}$ is likely dominated by transport of biomass burning plumes from the eastern grasslands (Ballesteros-González et al., 2020). While most of the anthropogenic sources are located near the Bogotá urban footprint over the Andes.

Those two distinct regimes appear related to the topographic features of the domain, with the region of overestimation located on the low-lands east of the Andes mountain range.

When we restrict the analysis to the urban area of Bogota, InMAP base $PM_{2.5}$ had a −12.9 % relative error, equivalent to a mean bias of $-2.0\,\mu g\,m^{-3}$, and a RMSE of 2.04 $\mu g\,m^{-3}$. When analyzed in a scatter plot, the InMAP fields are strongly linearly correlated with those of WRF-Chem, with a Pearson correlation coefficient of 0.99 (for the urban area of Bogotá) and 0.91 for the entire D03 domain. Overall, the base case simulation by InMAP is accurate over the specified domain.

3.3 InMAP sensitivity

The marginal fine particle concentration fields, $\Delta PM_{2.5}$, for each of the scenarios from Table 2 are shown in Fig. 4. These marginal concentration fields can be regarded as the model sensitivity to the emission reductions that define each scenario. InMAP sensitivities were significantly larger than those of WRF-Chem, and the magnitude of the sensitivity of aerosol components to emissions was strongly dependent on the type of emission reduction scenario. For the RPM-100 scenario, which exclusively involves reductions in primary PM emissions, the ratio of InMAP to WRF-Chem sensitivity for grid-cells within the city limits was on average two times larger than that of the full CTM, with a mean ratio of 2.0 and a confidence interval (C.I.) of 1.81 to 2.35. The mean ratios reported in this manuscript were estimated as the mean of the ratios at each grid-cell, and the confidence intervals, based on Student't t distribution, were computed for a 0.95 confidence level.

The sensitivities for non-primary PM components vary significantly between InMAP and the full CTM. Particularly critical in our analysis was the large overestimation in the sensitivity of particulate nitrate and secondary organic aerosol (SOA) to precursor emissions. This was most notorious in the *Diesel-100* scenario, where the mean ratio of the model-to-model sensitivity was 5.0 (C.I. 4.22–5.79), implying a more severe overestimation compared with the simpler RPM scenario. The additional sensitivity was driven mostly by an excessive secondary aerosol yield in InMAP. Noticeably, in all the scenarios analyzed, the overestimation of the

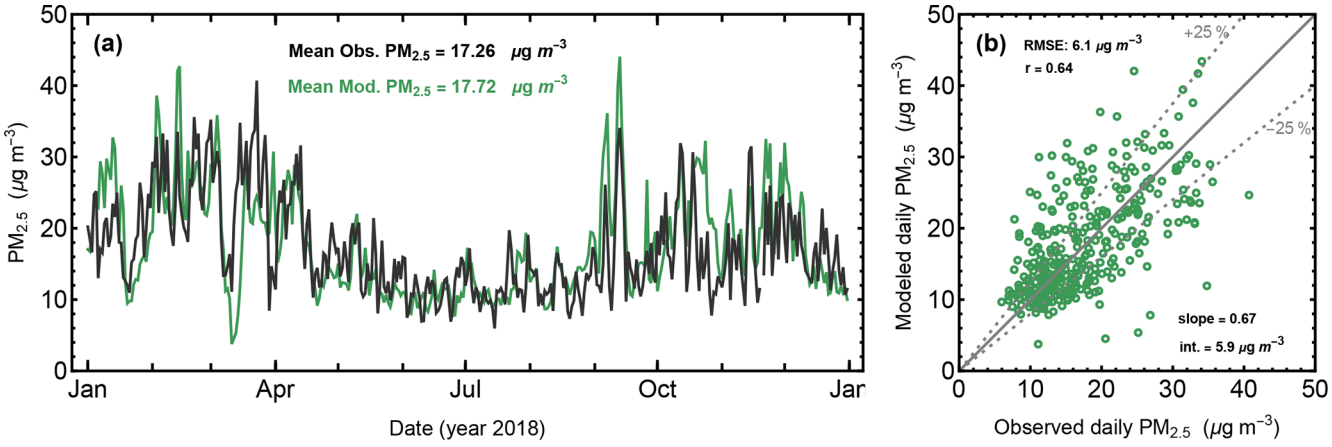


Figure 1. **(a)** Time series of modeled (green) and observed (black) daily surface $PM_{2.5}$ concentration in the city of Bogota for 2018. **(b)** Scatter plot of observed and modeled daily $PM_{2.5}$ concentration. The root mean square error (RMSE) and Pearson correlation (r) are included, as well as the slope and intercept of a simple linear regression. The observed values are daily means from the 11 reference air quality monitoring sites that had sufficient valid $PM_{2.5}$ daily data.

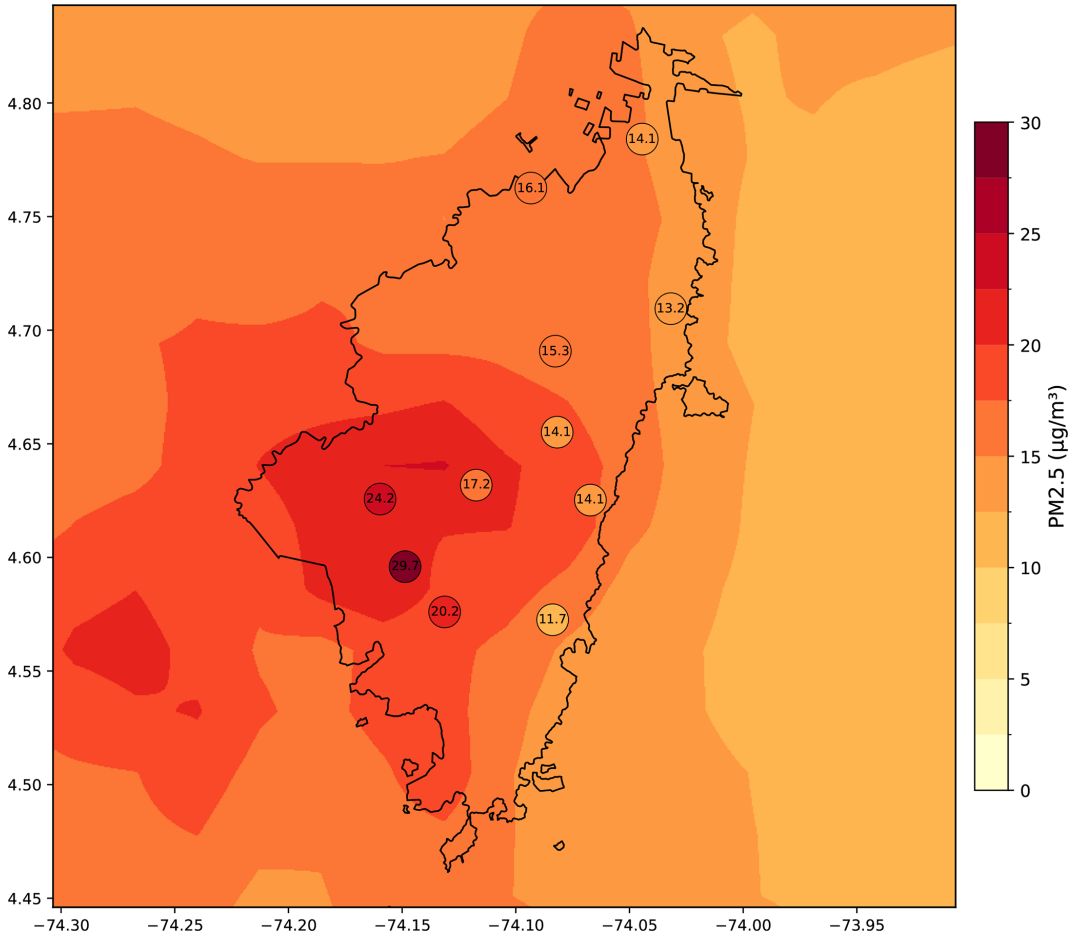


Figure 2. Annual mean spatial distribution of simulated $PM_{2.5}$ in a portion of the innermost domain containing the urban area of the city. The urban footprint is shown as the black contour. The observed annual mean $PM_{2.5}$ at the available air quality monitoring stations is also shown.

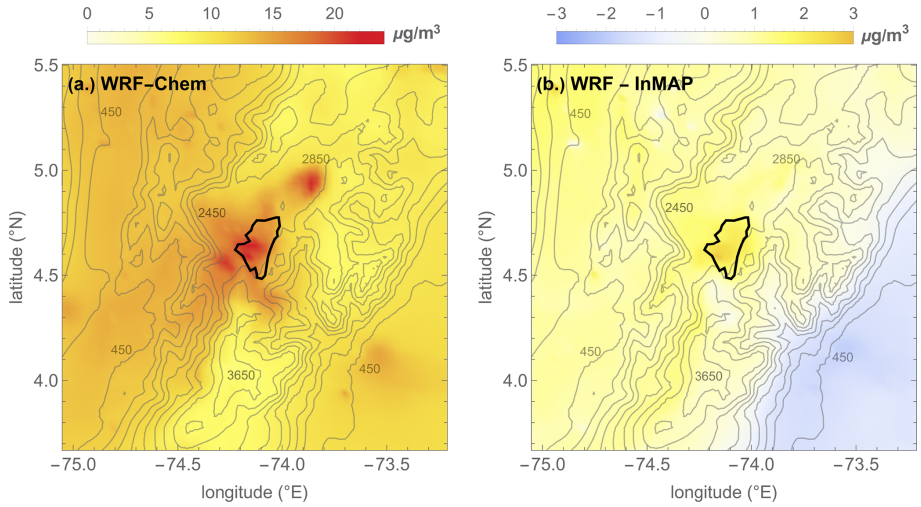


Figure 3. (a) Annual mean $PM_{2.5}$ (in $\mu g\,m^{-3}$) for the inner most domain modeled with WRF-Chem, and **(b)** difference in annual mean $PM_{2.5}$ (in $\mu g\,m^{-3}$) between WRF-Chem and InMAP base case. Positive (negative) values in panel **(b)** indicate underestimation (overestimation) by InMAP. The thick black contour depicts the urban area of Bogota. Terrain height contours in 400 m intervals are included in the graphic showing the complex topographic features of the domain.

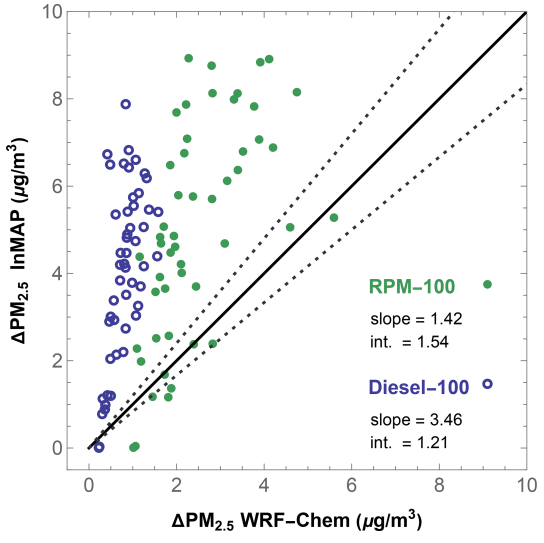


Figure 4. Scatter plot of the marginal $PM_{2.5}$ concentrations calculated with the full chemical transport model WRF-Chem ($\Delta PM_{2.5}$ WRF-Chem) and with the InMAP model ($\Delta PM_{2.5}$ InMAP). The data shown is for the test scenarios in which resuspended dust emissions were removed (RPM-100) and for the one in which all diesel emissions from mobile sources were removed (Diesel-100). Only those cells within the city limits are included.

primary PM sensitivity was close to a factor of 2 relative to the WRF-Chem sensitivity. Based on the consistency of this number, we hypothesize that in our area of study InMAP's atmospheric transport efficiency is limited, causing that most of the emitted particle mass remains near the surface layer. Therefore, for the most complex emission reduction scenarios, the overestimation in marginal $PM_{2.5}$ seems to be driven by the reduced transport (roughly a factor of 2), and another overestimation factor from the overproduction of secondary aerosol species, mainly particulate nitrate and SOA.

The resulting marginal concentration fields from InMAP are moderately linearly correlated with those from WRF-Chem, with Pearson correlation coefficients of 0.60 for the RPM-100 test scenario and 0.59 for the Diesel-100 scenario. When linear regressions are applied to both scenarios we obtain slopes of 1.42 (C.I. 0.88–1.95) for RPM-100 and 3.46 (C.I. 2.1–4.8), and a non-zero offset (Fig. 4), showing that the model-to-model sensitivities might not be brought to agree entirely by a simple proportional scaling. Therefore, despite the overestimation in the marginal concentration from emission reductions, the spatial patterns produced by InMAP are consistent with those of the full CTM. This suggests that InMAP can be used to carry out order of magnitude assessments of the spatial footprint of specific emission reduction scenarios, and, if paired with demographic and health data, estimate the associated health benefits derived from that distribution of emission cuts (Sect. 3.4). In the moderate *10 %-diesel* the modeled marginal reductions were much smaller, with average marginal changes of $0.12\,\mu g\,m^{-3}$ for WRF-Chem. The mean ratio of sensitivities for that reduction scenario was 3.59 (C.I. 3.01–4.16), showing a lower relative overestimation of SOA mass compared to the *no-diesel* scenario. This suggests that scenarios with strong reduction in gas-phase precursors could be challenging for the InMAP model, as has been reported in other studies (e.g., Thakrar et al., 2022). The difference in the model-to-model sensitivity shown between the moderate *10 %-diesel* and the *no-diesel* scenarios highlights how complex interactions in the atmosphere that can cause non-linear responses are intrinsically

challenging for models like InMAP that respond linearly to emission reductions. Further analysis of the gas-to-particle partitioning parameters used in the model could be revised in future studies.

3.4 InMAP application: derivation of benefits

To showcase a potential application of InMAP-Bog for quickly scanning the emission configuration space, we carried out a simple cell-by-cell reduction experiment. We applied a $1\,\mathrm{t\,yr^{-1}}$ primary $PM_{2.5}$ emission reduction in each cell within the urban footprint of Bogotá, one at a time. In this example 78 scenario simulations were carried out. The procedure consisted on creating the corresponding 1-cell synthetic reduction scenarios, repeatedly executing InMAP with that input, and storing the output marginal concentrations. For each run, we defined the *benefits* as the total change in population exposure (the product of population and concentration reduction) at the receptor cells. This is, if emissions are reduced in cell k, then, the benefits, ΔPM_{exp} per unit tonne, associated to that cell is computed as

$$\Delta PM_{exp_k} = \sum_j Pop(j)\Delta PM_{j,k} \quad (2)$$

where $\Delta PM_{j,k}$ is the annual mean reduction in $PM_{2.5}$ at the receptor cell j derived from the reduction in emission in cell k, and $Pop(j)$ is the population in the receptor cell. If paired with spatially resolved baseline incidence of health outcomes and using the appropriate concentration-response function parameter, ΔPM_{exp_k} is proportional to the avoided health endpoints. In this example, avoided mortality or morbidity were not calculated as the spatially resolved baseline data was not available for the entire domain. However, the resulting distribution of benefits can point policy makers to the locations were emission cuts could provide the largest health benefits. The result from this analysis is shown in Fig. 5. The analysis exemplifies how the locations of the grid-cells that achieve the most benefits per unit emission reduction (Fig. 5b), do not necessarily coincide with those were emissions are the largest (Fig. 5a).

Even when taking into account the associated uncertainties and biasses of this calculation, policy makers can scan multiple such source-receptor relationships to identify key areas for intervention within the city. Once a general area has been identified, other scale-appropriate tools should be applied at the relevant scale (e.g., Resler et al., 2017; Maronga et al., 2020).

4 Discussion

As discussed earlier, the overestimation of sensitivities to emissions exhibited by InMAP compared to the comparable full CTM runs are likely attributable to limitations in the representation of vertical mixing and to the necessary simplifications implied in the model for computing the partitioning of gases to secondary aerosols. However, as discussed elsewhere (e.g., Thakrar et al., 2022), despite the relatively large uncertainties expected from applying RCMs, the outputs can still provide policy-relevant information. Caution should be exercised if solely basing policy decisions based on results from a single simplified model. If urban-scale policies involve specific interventions, higher-resolution models (e.g., Maronga et al., 2020), together with other criteria should be considered. The results shown in this work suggest that further development of the diagnostic equations of the errors associated with vertical mixing and partitioning coefficients, could be directly corrected within the InMAP code, but would require substantial work and testing in many different settings.

To our knowledge, there are no other implementations of RCMs in South America, and there is no clear benchmark to compare our results against. The NMB reported in our scenario simulations are larger than those reported in other model-to-model comparisons (Wu et al., 2021; Tessum et al., 2017, e.g.,). Large biases in the marginal concentration changes are not uncommon in other studies using InMAP. For instance, (Thakrar et al., 2022) reports NMB of $+120\,\%$ globally and up to $+371\,\%$ at the regional level in their model-to-model comparison. As the authors argue, given that damages per tonne emitted can vary by orders of magnitude across space, tools like RCMs can still provide order of magnitude estimates that can inform policy decisions.

The moderate linear association shown for marginal concentrations for primary particle emissions reductions scenarios suggest that InMAP-Bog can be of use to prioritize areas for emission primary particle reductions (such as resuspended matter control strategies). The policy-value of the setup reported here is that InMAP, once built, could be quickly used to explore spatial patterns of emission reductions or can help identify the most influential cells in reducing, for example, overall population exposure to $PM_{2.5}$ in the domain. Therefore, our work shows a pathway for practical applications of this type of RCMs.

Other RCM architectures, such as the statistical approaches adopted in some tools, have shown smaller biases than those of the more physically based approaches such as the one used in InMAP (e.g., Thunis et al., 2018). However, the lack of CTM and RCM applications in regions like Latin America precludes the possibility of determining the relative performance of different architectures for the specific challenges of the region. Therefore, future development and application of RCMs in regions such as Latin America were these tools are needed the most, could focus on implementing and comparing multiple RCMs with different architectures.

The spatial distribution of concentration shown in Fig. 3 suggests that the high-spatial resolution is necessary as two dominant patterns are observed. At the largest-scale of D03 ($\sim 100\,\mathrm{km}$) the simulation shows a gradient between the lowlands in the east and the highlands in the western margin of the domain. At smaller scales ($\sim 10\,\mathrm{km}$), comparable to

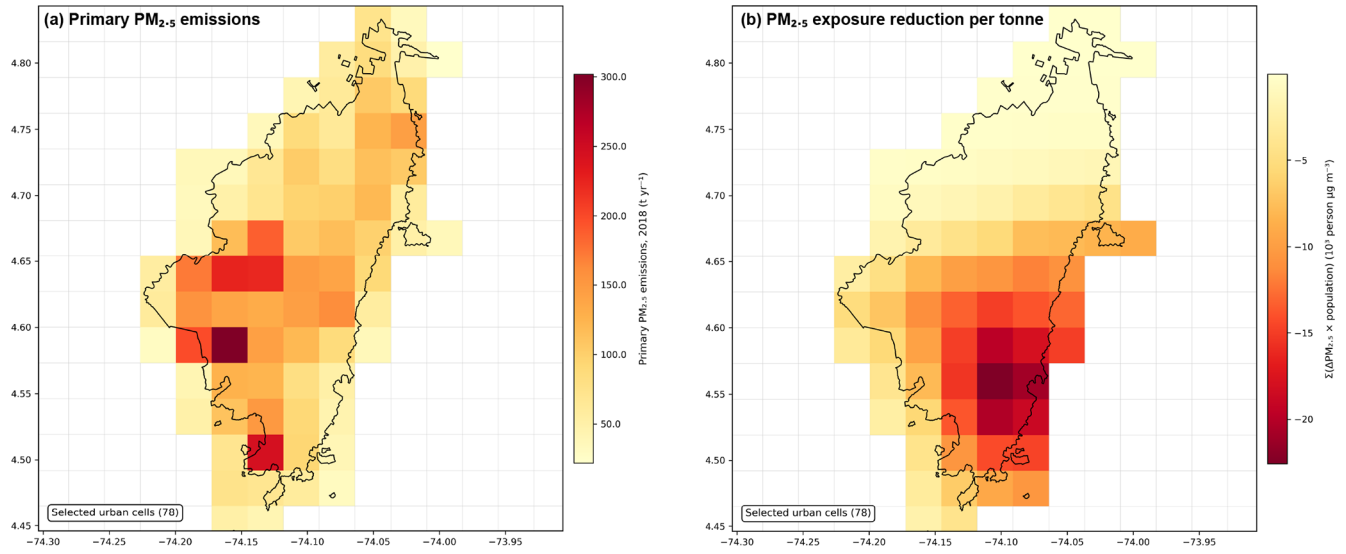


Figure 5. (a) Base scenario primary $PM_{2.5}$ emissions in Bogotá, and **(b)** benefits, expressed as exposure reduction within the city per tonne of primary $PM_{2.5}$ reduced in a year

the East-West width of the urban footprint, the simulation captures the intra-urban gradient between the most polluted Southwest and the cleaner Northeast. Such small-scale gradients would not be properly captured in coarser-scale simulations. The importance of this is maximized when the population density in the region is analyzed, as there is a clear spatial correlation between the observed (and modeled) Southwest to Northeast $PM_{2.5}$ concentration gradient, and population density (Fig. A1b). Therefore, accurately reproducing the observed intra-urban gradient is key to realistically represent population exposure, given the population density distribution. The influence of the regional transport of biomass burning plumes has a strong impact in the seasonality of air pollution, but does not seem to modify the intra-urban gradients seen in the air quality data.

Lastly, future applications of this type of CTM and RCM combination should be planned carefully, if they are to be transferred to decision makers, as the CTM step still has to be done with all the complexities and computational costs involved. Once built, InMAP wall-clock time is several orders of magnitude shorter than the required for a full CTM run. In our system, a desktop computer, a test scenario with in which emissions are reduced in just one cell took 14 min to run. Therefore, even with limited computing power, around 100 such scenarios can be run in one day. This facilitates the construction of source-receptor matrices quickly as demonstrated here. The storage requirements for InMAP input and output are also much smaller than that of the full CTM, with the output file size from each scenario using 648 kB. However, if access to high-performance computing is not available, the CTM step could be prohibitively time consuming. Each one-day of WRF-Chem inner-most domain (D03) simulation took around 8 h wall-clock time in the same system using 8 processors. Each one of WRF-Chem daily output files (with hourly output) for the D03 domain alone occupies 2.69 GB of storage, and the full-year simulation encompasses nearly 1TB of data. The full year simulation took, overall, several months to be completed using four computers with 8 processors and 128 GB memory each. Therefore, whenever possible, existing high-quality CTM runs should be leveraged, and further studies could explore the possibility to simulate shorter periods with the CTM when comparing marginal concentration changes for scenario testing.

5 Conclusions

We implemented the reduced complexity model InMAP at a spatial resolution of 3 km × 3 km using a detailed atmospheric chemical transport simulation with the WRF-Chem model. The WRF-Chem base simulation was shown to meet high quality criteria when compared to observed $PM_{2.5}$ concentrations at the city-scale, with low biases, and showing similar variability at daily and seasonal scales. The simulated spatial patterns reproduce the observed intra-urban concentration gradients. In the baseline simulation, we explored the application of weekly activity patterns, which improved the ability of the model to capture the observed variability of $PM_{2.5}$ fields at the city scale.

In addition to evaluating InMAP's baseline run, we also tested InMAP sensitivity by comparing it with a set of three emission reduction scenarios that were also simulated with the WRF-Chem chemical transport model. Overall, we found that InMAP overestimated marginal $PM_{2.5}$ for all emission reduction scenarios considered. For settings in which only primary PM was reduced, with no gas-phase species changes,

InMAP predicted twice as large concentration reductions compared to WRF-Chem.

For more complex emission reduction scenarios involving also reduction in gas-phase emissions, InMAP overestimated $PM_{2.5}$ concentrations more severely. The driver in InMAPs overestimated $PM_{2.5}$ sensitivity in the scenarios involving gas-phase precursors was a large overestimation of secondary organic aerosols and particulate nitrate. For those cases, the model-to-model marginal concentration changes showed a moderate linear association, suggesting that the spatial footprint of InMAP's response can help guide emission reduction scenarios.

Despite some of the limitations detected in this study, the computational efficiency of the reduced complexity model and the linear relation of its sensitivities to those of the full CTM, suggests this tool could be useful for researchers or policy makers to quickly scan through a large number of potential emission reductions scenarios sorting them based on its efficacy in reducing exposure. This allows the exploration of a large space of potential scenarios, and to quickly narrowing it down to those with the largest potential benefits. Once the most promising scenarios are selected, a few simulations with the full CTM can be carried out to better quantify the actual concentration and health-related benefits expected from a given emission reduction policy. However, for regions were computational resources are limited, any further CTM use would substantially increase the time involved in impact estimates.

Appendix A: Model configuration and description of nested domains

The WRF-Chem model configuration was selected based on the skill shown on previous modeling studies over the same region (e.g., Ballesteros-González et al., 2020). The set of parameterization and physics option were already provided in Sect. 2.1.2.

To achieve sufficiently high spatial resolution for meaningful urban-scale modeling for the city of Bogota we configured the WRF-Chem model with three nested domains of increasing spatial resolution (Fig. A1a). The domains centered in the city of Bogota (lat. 4.666, – long. −74.098) have a horizontal resolution of 27×27 km (120×120 grid cells), 9×9 km (126×126 grid cells), and 3×3 km (69×69 grid cells) for domain 1 (D01), domain 2 (D02), and domain 3 (D03), respectively. Due to its relevance for urban-scale analysis, only the fields resulting from the highest resolution domain, D03, were used in this work. For domain D03, population is highly concentrated within the urban footprint of the city, with population density exceeding 20 000 people per square km (Fig. A1b) and some urban sprawl to the North and West of the city. However, the rest of the domain is relatively sparsely populated. Simulations were conducted for the entire year of 2018 for the three domains. The outermost domain (D01) is driven laterally by the meteorological and chemical-species fields from global chemical transport models, as described in the main text. The simulations for all domains were split in 3-month batches, corresponding to January–March, April–June, July–September, and October-December. Given the large domain size for D01 (roughly $3240\,\text{km} \times 3240\,\text{km}$) each 3-month batch was initialized with the global model fields three days prior to the initial analysis date, allowing for 72 h of spin-up time. Numerical experiments for the three domains shared the same physical parameterizations.

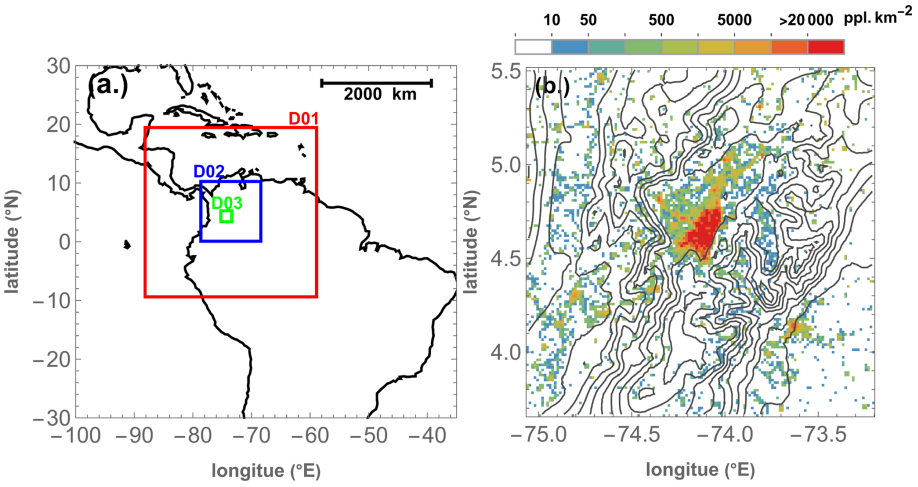


Figure A1. **(a)** Geographic location of the three modeling domains used in this study in a latitude-longitude representation. Each nested domain has increasingly higher spatial resolution. Although the simulation was carried out for the 3 domains, only the results from the innermost (D03) are reported in this study. **(b)** Population density (in per km^2) and terrain elevation contours for D03.

Appendix B: Local emissions and source activity patterns

B1 Weekly activity variations

To account for significant variations in mobile source activity patterns throughout the year, we used the public transport system weekly ridership data reports as a proxy of mobile source activity. These reports are made publicly available by the city's public transport authority. The activity factor we introduced in our emissions was defined such that it represents deviations from the average ridership, which was set to 1 (Fig. B1).

The sharp activity variations are well explained by some societal factors. The education sector (from elementary schools to universities) typically have holiday breaks in December–January and June–July. Additionally, many companies and government agencies have holidays from mid-December to mid-January. The ridership data captures the above described patterns, exhibiting large departures from the annual mean values for specific periods. On average, daily ridership in the public transport system for 2018 was 2.3 million trips. Minimum ridership is observed in the first week of the year (with 1.35 million trips per day) with a similar decline in the last week of the year. There is a decrease in activity during the religious holiday Easter, as Thursday and Friday of that week are national public holidays. We consider this approach as a good proxy of activity, and the method potentially useful for researchers elsewhere aiming to capture day-to-day and week-to-week variations in air quality simulations. Additionally, because of the strong daily activity variations within city, we also applied specific activity factors for weekdays, Saturdays, and Sundays (including public holidays).

B2 Local and global emission merging

The spatial scale of global emissions inventories is not suitable for urban-scale modeling applications. To circumvent that issue we used emissions from the local atmospheric emission inventory for the city limits of Bogota for year 2018, at 1x1km resolution, and merged it with the global emission inventory for those areas in D03 outside the city. If $B_{i,j}$ is the fraction of a given 3×3 km grid cell that has local emission data (i.e., the fraction of that grid cell that overlaps with the gridded local emission inventory of Bogota), then we merged the global and local emissions using

$$E_{i,j} = B_{i,j} \times E^{\text{local}}_{i,j} + \left(1 - B_{i,j}\right) \times E^{\text{global}}_{i,j} \quad \text{(B1)}$$

where $E^{\text{local}}_{i,j}$ is the flux of emissions from the local emission inventory for grid cell i, j, and $E^{\text{global}}_{i,j}$ is the flux for that cell from EDGAR. In this way, for model grid cells entirely inside the domain of the local emission inventory we use local emissions. For those cells completely outside the domain of the local emission inventory, then we use the global emissions. For the handful of *boundary* cells that partially overlap with the local emission inventory, then the emissions of both are combined according to Eq. (B1).

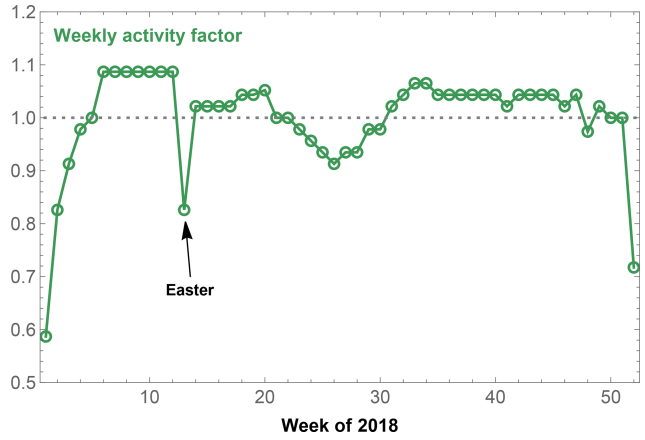


Figure B1. Normalized weekly activity factor, f_w, for mobile sources as inferred from ridership data from the city's public transport system. The factor was defined such that annual-mean activity is set to 1. When $f_w > 1$ it implies above-average activity, while $f_w < 1$ indicates below-average activity levels.

Appendix C: Statistical evaluation of the model skill for $PM_{2.5}$

We applied multiple metrics to assess the model skill to represent fine particulate ($PM_{2.5}$) spatial and temporal distributions for the city of Bogota. Modeled daily mean $PM_{2.5}$ for the entire year 2018 were compared to available observations over the same period. There were 11 air quality monitoring sites with valid data (i.e., $> 75\,\%$ of valid data) to carry out the comparison for the simulation period. The metrics include:

$$\mathrm{NMB} = 100 \times \frac{\sum (M_j - O_j)}{\sum O_j} \tag{C1}$$

$$\mathrm{NME} = 100 \times \frac{\sum |M_j - O_j|}{\sum O_j} \tag{C2}$$

where M_j are model outputs and O_j are observations for a specif location j, and the summation is carried out over time, in this case, over model and observed daily-mean $PM_{2.5}$ concentrations. The results are shown in *soccer-goal* plots (NMB and NME metrics) and Taylor diagrams (modeled and observed standard deviation, and correlation coefficient, ρ). In this way, we assessed temporal correlation metrics, variability metrics, and bias-related metrics (Fig. C1).

C1 City-wide analysis

For this analysis we pooled together the daily-mean $PM_{2.5}$ concentrations from all the available monitoring sites to create a city-mean $PM_{2.5}$ time series. To create a comparable dataset from the model output, we averaged all the daily-means from the specific grid cells within the urban footprint of the city. At the city-mean scale, the model meets the performance goals for NMB and NME as specified in Emery et al. (2017), with NMB of $+2.7\,\%$ and NME of $27\,\%$. The Pearson correlation coefficient was 0.64, which is higher than the criteria of 0.4, but falls short of the *goal* performance threshold of 0.7. Results for the city-wide analysis are shown as the black circles in Fig. C1. Our analysis was carried out for the 365 paired model and observed daily means.

C2 Intra-city variations

We evaluated the same model performance metrics for each individual monitoring site to determine the model's ability to capture intra-city variations in air quality fields. Figure C1b shows the NMB and NME for the model when evaluated against observations. The model met the bias and error criteria for the 11 stations analyzed Emery et al. (2017). Furthermore, The stricter *goals* where met for 4 out of 11 stations. Furthermore, as seen in Fig. C1a, the model performance for 10 out of 11 monitoring sites met the correlation coefficient criteria $\rho > 0.4$, with the lone exception of an industrial monitoring site, which shows a distinctly different temporal structure to the other monitoring sites. The assessment of model performance reported here suggests the model configuration is capable of capturing intra-city gradients and temporal variations in this urban setting. The locations and annual mean $PM_{2.5}$ concentrations for the city's air quality monitoring sites is shown in Table C1.

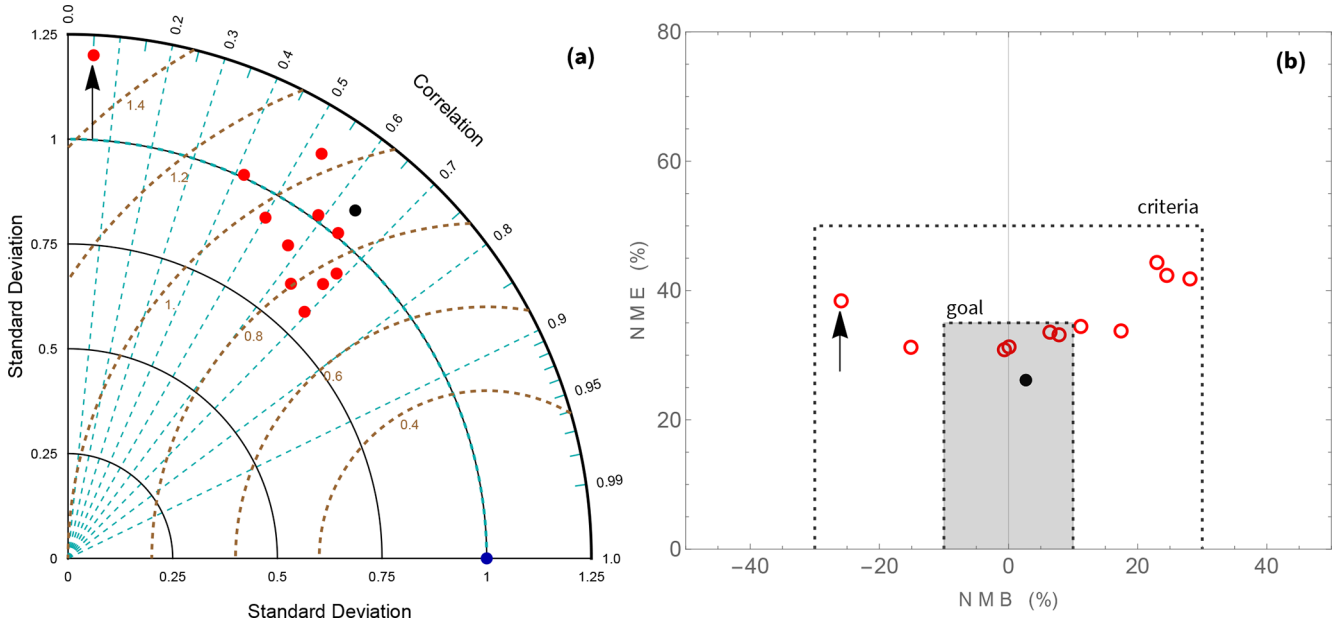


Figure C1. (a) Taylor diagram for modeled and observed daily $PM_{2.5}$ data for the 11 stations with valid data (red points). The black circle represents the city-mean $PM_{2.5}$ timeseries. In this diagram, the x axis is the standard deviation (SD) normalized by the SD of the observed data. The dashed circles are the centered RMSE, also normalized by the observed SD. **(b)** *Soccer-goal* plot showing the Normalized Mean Bias (NMB) and Normalized Mean Error (NME) for the same data set. The *goal* benchmark region is shaded in gray. The arrow is pointing to station S1, which was the only site with a correlation coefficient lower than the 0.4 criteria.

Table C1. Air quality monitoring site information for those with valid $PM_{2.5}$ data for 2018. Stations are sorted in order of decreasing annual mean $PM_{2.5}$ concentration for the period. We include the Station ID, Annual mean $PM_{2.5}$ concentration, station location in lat. lon. coordinates, and the type of station.

Station ID	Annual mean $PM_{2.5}$ ($\mu g\,m^{-3}$)	Lon. Degrees	Lat. Degrees	Type
Carvajal – Sevillana (S1)	29.7	−74.1487	4.59591	Industrial
Kennedy	24.2	−74.1597	4.62567	Background
Tunal	20.2	−74.1313	4.57599	Background
Puente Aranda	17.2	−74.1174	4.63182	Industrial
Suba	16.1	−74.0934	4.76255	Background
Las Ferias	15.3	−74.0826	4.69076	Traffic
Min. Ambiente	14.1	−74.0672	4.62523	Traffic
Guaymaral	14.1	−74.0444	4.7841	Background
CAR	14.1	−74.0818	4.65511	Background
Usaquen	13.2	−74.0318	4.70946	Background
San Cristobal	11.7	−74.0838	4.57256	Background

Appendix D: Statistical evaluation of the model meteorological fields

We tested the model performance by comparing some meteorological variables against available data using widely used performance criteria (Emery et al., 2001). The ground-based data was was relatively scarce, as only seven stations had enough valid data (i.e., $\geq 75\,\%$ of hourly data) for temperature, nine for wind-speed, and seven for wind direction.

The temperature fields are consistent with observations, and follow the characteristic patterns observed in equatorial regions, where the amplitude of the observed (and modeled) diurnal cycle is larger than the weak monthly variations (Fig. D1). The model mean error for most stations fulfills the criteria, but the IOA does not (Table D1). The modeled temperatures are biased low, which could be due to excessive radiational cooling due to the challenge of capturing cloudiness correctly.

Wind speeds in the city are low, with means rarely exceeding $2.5\,\mathrm{m\,s^{-1}}$. The diurnal profile exhibits low wind speeds for the early morning hours, ranging between $1.0\,\mathrm{m\,s^{-1}}$ (range of 0.6 to $1.8\,\mathrm{m\,s^{-1}}$) and reaching a peak afternoon speeds of 2 to $4\,\mathrm{m\,s^{-1}}$ (Fig. D2). Overall, the model struggles to capture these low-wind conditions, showing stronger than observed winds in the afternoon. The RMSE for modeled WS is low and meets the criteria for all stations, however, this should be interpreted carefully as wind-speeds overall are low, implying large relative errors. Evaluation of model performance regarding wind direction is summarized in Table D1. For the available observations, the model meets the mean bias criteria for three stations, but the mean errors exceed the benchmark for all stations. Other studies have reported the difficulty in capturing the complex wind patterns in the city (Nedbor-Gross et al., 2017).

Table D1. Modeled temperature (T) and wind speed (WS) performance metrics. MB = mean bias, ME = mean error, RMSE = root mean square error, and IOA is the index of agreement. Those in bold face reach the performance criteria.

Station ID	Annual mean T (°C)	MB (°C) $\leq \pm 0.5$	ME (°C) ≤ 2	IOA (–) ≥ 0.7
Carvajal – Sevillana	15.46	−1.61	**1.64**	0.41
Centro de Alto Rendimiento	14.72	**−0.27**	**0.83**	0.44
Guaymaral	14.48	−1.09	**1.18**	0.48
Las Ferias	14.15	**0.33**	**0.80**	0.50
Puente Aranda	14.20	**0.28**	**0.70**	0.57
San Cristobal	13.10	−1.80	**1.81**	0.42
Suba	14.43	−2.46	2.47	0.34
Station ID	Annual mean WS ($m\,s^{-1}$)	MB ($m\,s^{-1}$) $\leq \pm 0.5$	RMSE ($m\,s^{-1}$) ≤ 2.5	IOA (–) ≥ 0.6
Carvajal – Sevillana	1.97	0.79	**1.39**	**0.60**
Centro de Alto Rendimiento	1.20	**−0.07**	**0.54**	0.53
Kennedy	2.28	**−0.12**	**0.81**	**0.67**
Las Ferias	1.64	**−0.09**	**0.65**	**0.63**
Puente Aranda	2.25	−1.03	**1.33**	0.42
San Cristobal	1.51	1.43	**2.22**	0.22
Suba	1.37	1.27	**1.47**	0.52
Tunal	1.24	0.93	**1.30**	0.23
Usaquen	1.65	1.23	**1.60**	0.44
Station ID	Annual mean WD (degrees)	MB (°) $\leq \pm 10°$	ME (°) $\leq 30°$	– –
Carvajal – Sevillana	158.4	**0.3**	53.3	–
Centro de Alto Rendimiento	40.5	**−4.1**	86.4	–
Puente Aranda	237.2	**−3.7**	71.5	–
San Cristobal	91.5	37.7	57.5	–
Suba	35.4	42.6	113.9	–
Tunal	192.2	-28.8	76.3	–
Usaquen	122.7	27.5	47.6	–

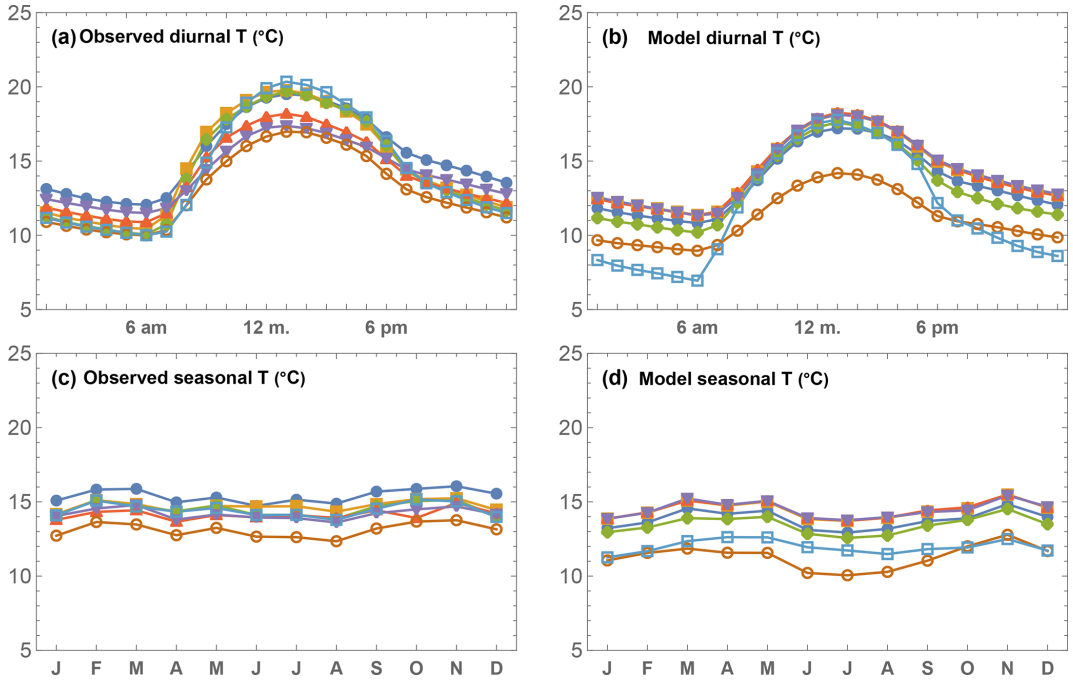


Figure D1. **(a)** Observed diurnal temperature profile and **(b)** modeled diurnal temperature profile. **(c)** Observed monthly mean temperature and **(d)** modeled monthly mean temperature.

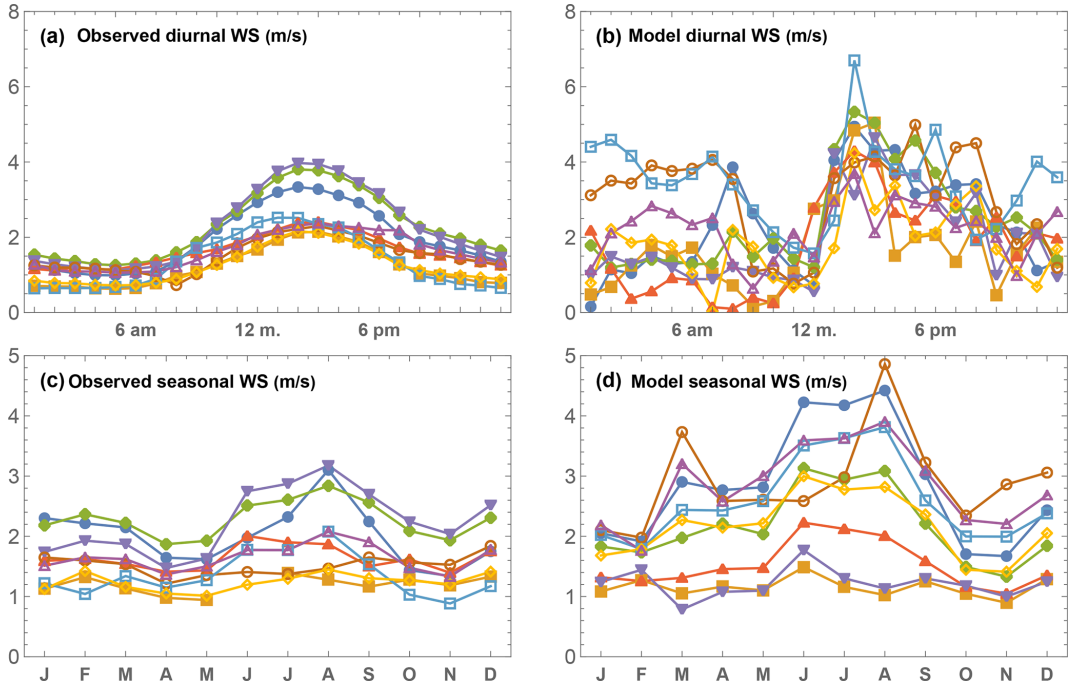


Figure D2. **(a)** Observed and **(b)** modeled diurnal wind-speed profile. **(c)** Observed and **(d)** Modeled monthly mean wind-speed.

Appendix E: WRF-Chem variables used in InMAP

Table E1. WRF-Chem variable names and their use in InMAP. The list presented here is identical to the one reported in Table S1 of the study describing InMAP first implementation (Tessum et al., 2017).

WRF-Chem variable	Description	Use in InMAP
hc5, hc8, olt, oli, tol, xyl, csl, cvasoa1, cvasoa2, cvasoa3, cvasoa4	Anthropogenic VOCs, SOA precursors	VOA/SOA partition
asoa1i, asoa1j, asoa2i, asoa2j, asoa3i, asoa3j, asoa4i, asoa4j	Antrhopogenig SOA	VOA/SOA partition
iso, api, sesq, lim, cvbsoa1, cvbsoa2, cvbsoa3, cvbsoa4	biogenic VOCs, SOA precursors	
bsoa1i, bsoa1j, bsoa2i, bsoa2j, bsoa3i, bsoa3j, bsoa4i, bsoa4j	biogenic SOA	
no, no2	NO_x	NO_x/pNO_3 partition
no3ai, no3aj	Particulate Nitrate	NO_x/pNO_3 partition
so2, sulf	SO_2 and sulfate	SO_x/pSO_4 partition
so4ai, so4aj	particulate SO_4	SO_x/pSO_4 partition
nh3	Ammonia	NH_3/pNH_4 partition
nh4ai, nh4aj	Particulate Ammonia	NH_3/pNH_4
PM2_5_DRY	$PM_{2.5}$	Model evaluation
U, V, W	wind components	Advection and Mixing
PBLH	Planetary Boundary Layer Height	Turbulent Mixing
PHB and PH	Base geopotential and its perturbation	Layer heights
HFX	Surface Heath Flux	Dry deposition and Mixing
UST	Friction velocity	Dry deposition
T	Temperature	Reaction rates
PB, P	Pressure and perturbation pressure	Reaction rates
ho, h2o2	Radicals	Reaction rates
LU_INDEX	Land Use Index	Turbulent mixing
QRAIN	Rain water mixing ratio	Wet deposition
CLDFRA	Cloud fraction	Dry deposition
QCLOUD	Cloud water mixing ratio	Reaction rates
ALT	Inverse air density	Conversion factor
SWDOWN, GLW	Downward radiation at surface	Dry deposition

Code and data availability. The source code, configuration files, and the preprocessed *.gob* file for the InMAP model as implemented in this paper, as well as the input data sets for the scenarios described here are archived on a data repository under DOI https://doi.org/10.5281/zenodo.19654866 (Morales Betancourt et al., 2026). Similarly, the source code and configuration files for WRF-Chem version 3.9.1, as well as surface-level daily means for the WRF-Chem simulation used in this manuscript are archived on a data repository under DOI https://doi.org/10.5281/zenodo.19655777 (Rojas Neisa et al., 2026). The three dimensional, hourly WRF-Chem fields are not archived, as their size is prohibitively large. Ground air pollution and meteorological data is available for download from the Air Quality Monitoring Network from Bogotá at https://rmcab.ambientebogota.gov.co/report/MonitorReport (last access: 2 October 2026).

Author contributions. DRRN: Conceptualization, Investigation, Software, Visualization, Writing – review and editing. AP: Conceptualization, Investigation, Writing – review and editing, Formal analysis. SEC: Investigation, Writing – review and editing. IR: Investigation, Visualization. RMB: Conceptualization, Methodology, Writing – Original Draft, Investigation, Visualization, Funding acquisition. Simulations were designed by all co-authors and were carried out and analyzed by DRRN, and AP.

Competing interests. The contact author has declared that none of the authors has any competing interests.

Disclaimer. Publisher's note: Copernicus Publications remains neutral with regard to jurisdictional claims made in the text, published maps, institutional affiliations, or any other geographical representation in this paper. The authors bear the ultimate responsibility for providing appropriate place names. Views expressed in the text are those of the authors and do not necessarily reflect the views of the publisher.

Review statement. This paper was edited by Ulas Im and reviewed by Martin Otto Paul Ramacher and one anonymous referee.

Financial support. This study was partially funded by the Center for Environmental Research (CIIA) from Universidad de los Andes.

References

Ackermann, I. J., Hass, H., Memmesheimer, M., Ebel, A., Binkowski, F. S., and Shankar, U.: Modal aerosol dynamics model for Europe: development and first applications, Atmos. Environ., 32, 2981–2999, https://doi.org/10.1016/S1352-2310(98)00006-5, 1998.

Ahmadov, R., McKeen, S. A., Robinson, A. L., Bahreini, R., Middlebrook, A. M., de Gouw, J. A., Meagher, J., Hsie, E.-Y., Edgerton, E., Shaw, S., and Trainer, M.: A volatility basis set model for summertime secondary organic aerosols over the eastern United States in 2006, J. Geophys. Res.-Atmos., 117, https://doi.org/10.1029/2011JD016831, 2012.

Appel, K. W., Napelenok, S. L., Foley, K. M., Pye, H. O. T., Hogrefe, C., Luecken, D. J., Bash, J. O., Roselle, S. J., Pleim, J. E., Foroutan, H., Hutzell, W. T., Pouliot, G. A., Sarwar, G., Fahey, K. M., Gantt, B., Gilliam, R. C., Heath, N. K., Kang, D., Mathur, R., Schwede, D. B., Spero, T. L., Wong, D. C., and Young, J. O.: Description and evaluation of the Community Multiscale Air Quality (CMAQ) modeling system version 5.1, Geosci. Model Dev., 10, 1703–1732, https://doi.org/10.5194/gmd-10-1703-2017, 2017.

Balasubramanian, S., Rojas-Mendoza, L., Barman, N., Wang, Y., Arub, Z., Saxena, S., Bekbulat, B., Bhardwaj, P., Marshall, J. D., Apte, J. S., and Venkataraman, C.: Preprint – Spatially Differentiated Multi-Sectoral Mitigation Strategies Needed to Reduce $PM_{2.5}$ Exposures in India, ChemRxiv [preprint], https://doi.org/10.26434/chemrxiv.15008347/v1, 2026.

Ballesteros-González, K., Sullivan, A. P., and Morales-Betancourt, R.: Estimating the air quality and health impacts of biomass burning in northern South America using a chemical transport model, Sci. Total Environ., 739, 139755, https://doi.org/10.1016/j.scitotenv.2020.139755, 2020.

Ballesteros-González, K., Espitia-Cano, S. O., Rincón-Caro, M. A., Rincón-Riveros, J. M., Perez-Peña, M. P., Sullivan, A., and Morales Betancourt, R.: Understanding organic aerosols in Bogotá, Colombia: In-situ observations and regional-scale modeling, Atmos. Environ., 284, 119161, https://doi.org/10.1016/j.atmosenv.2022.119161, 2022.

Bonilla, J. A., Aravena, C., and Morales-Betancourt, R.: Assessing Multiple Inequalities and Air Pollution Abatement Policies, Environ. Resour. Econ., 84, 695–727, https://doi.org/10.1007/s10640-022-00745-3, 2023.

Brauer, M., Freedman, G., Frostad, J., van Donkelaar, A., Martin, R. V., Dentener, F., v. Dingenen, R., Estep, K., Amini, H., Apte, J. S., Balakrishnan, K., Barregard, L., Broday, D., Feigin, V., Ghosh, S., Hopke, P. K., Knibbs, L. D., Kokubo, Y., Liu, Y., Ma, S., Morawska, L., Sangrador, J. L. T., Shaddick, G., Anderson, H. R., Vos, T., Forouzanfar, M. H., Burnett, R. T., and Cohen, A.: Ambient Air Pollution Exposure Estimation for the Global Burden of Disease 2013, Environ. Sci. Technol., 50, 79–88, https://doi.org/10.1021/acs.est.5b03709, 2016.

Burnett, R., Chen, H., Szyszkowicz, M., Fann, N., Hubbell, B., Pope, C. A., Apte, J. S., Brauer, M., Cohen, A., Weichenthal, S., Coggins, J., Di, Q., Brunekreef, B., Frostad, J., Lim, S. S., Kan, H., Walker, K. D., Thurston, G. D., Hayes, R. B., Lim, C. C., Turner, M. C., Jerrett, M., Krewski, D., Gapstur, S. M., Diver, W. R., Ostro, B., Goldberg, D., Crouse, D. L., Martin, R. V., Peters, P., Pinault, L., Tjepkema, M., van Donkelaar, A., Villeneuve, P. J., Miller, A. B., Yin, P., Zhou, M., Wang, L., Janssen, N. A. H., Marra, M., Atkinson, R. W., Tsang, H., Thach, T. Q., Cannon, J. B., Allen, R. T., Hart, J. E., Laden, F., Cesaroni, G., Forastiere, F., Weinmayr, G., Jaensch, A., Nagel, G., Concin, H., and Spadaro, J. V.: Global estimates of mortality associated with long-term exposure to outdoor fine particulate matter, P. Natl. Acad. Sci. USA, 115, 9592–9597, https://doi.org/10.1073/pnas.1803222115, 2018.

Chen, J. and Hoek, G.: Long-term exposure to PM and all-cause and cause-specific mortality: A systematic review and meta-analysis, Environ. Int., 143, 105974, https://doi.org/10.1016/j.envint.2020.105974, 2020.

Choma, E. F., Evans, J. S., Hammitt, J. K., Gómez-Ibáñez, J. A., and Spengler, J. D.: Assessing the health impacts of electric vehicles through air pollution in the United States, Environ. Int., 144, 106015, https://doi.org/10.1016/j.envint.2020.106015, 2020.

Clappier, A., Pisoni, E., and Thunis, P.: A new approach to design source–receptor relationships for air quality modelling, Environ. Model. & Softw., 74, 66–74, https://doi.org/10.1016/j.envsoft.2015.09.007, 2015.

Crippa, M., Janssens-Maenhout, G., Dentener, F., Guizzardi, D., Sindelarova, K., Muntean, M., Dingenen, R. V., and Granie, C.: Forty years of improvements in European air quality: regional policy-industry interactions with global impacts, Atmos. Chem. Phys., 6, 3825–3841, https://doi.org/10.5194/acp-16-3825-2016, 2016.

Donahue, N. M., Robinson, A. L., and Pandis, S. N.: Atmospheric organic particulate matter: From smoke to secondary organic aerosol, Atmos. Environ., 43, 94–106, https://doi.org/10.1016/j.atmosenv.2008.09.055, 2009.

Dudhia, J.: Numerical study of convection observed during the winter monsoon experiment using a mesoscale two-dimensional model, J. Atmos. Sci., 46, 3077–3107, https://doi.org/10.1175/1520-0469(1989)046<3077:NSOCOD>2.0.CO;2, 1989.

East, J., Montealegre, J. S., Pachon, J. E., and Garcia-Menendez, F.: Air quality modeling to inform pollution mitigation strategies in a Latin American megacity, Sci. Total Environ., 776, 145894, https://doi.org/10.1016/j.scitotenv.2021.145894, 2021.

Ek, M., Mitchell, K., Lin, Y., Rogers, E., Grunmann, P., Koren, V., Gayno, G., and Tarpley, J.: Implementation of Noah land surface model advances in the National Centers for Environmental Prediction operational mesoscale Eta model, J. Geophys. Res.-Atmos., 108, https://doi.org/10.1029/2002JD003296, 2003.

Emery, C., Tai, E., and Yarwood, G.: Enhanced meteorological modeling and performance evaluation for two Texas ozone episodes, Tech. rep., ENVIRON International Corporation, https://wayback.archive-it.org/414/20210529064218/https://www.tceq.texas.gov/assets/public/implementation/air/am/contracts/reports/mm/EnhancedMetModelingAndPerformanceEvaluation.pdf (last access: 16 November 2026), 2001.

Emery, C., Liu, Z., Russell, A. G., Odman, M. T., Yarwood, G., and Kumar, N.: Recommendations on statistics and benchmarks to assess photochemical model per-

formance, J. Air Waste Manage. Assoc., 67, 582–598, https://doi.org/10.1080/10962247.2016.1265027, 2017.

Emmons, L. K., Schwantes, R. H., Orlando, J. J., Tyndall, G., Kinnison, D., Lamarque, J.-F., Marsh, D., Mills, M. J., Tilmes, S., Bardeen, C., Buchholz, R. R., Conley, A., Gettelman, A., Garcia, R., Simpson, I., Blake, D. R., Meinardi, S., and Pétron, G.: The Chemistry Mechanism in the Community Earth System Model Version 2 (CESM2), J. Adv. Model. Earth Syst., 12, e2019MS001882, https://doi.org/10.1029/2019MS001882, 2020.

Fast, J. D., Gustafson Jr., W. I., Easter, R. C., Zaveri, R. A., Barnard, J. C., Chapman, E. G., Grell, G. A., and Peckham, S. E.: Evolution of ozone, particulates, and aerosol direct radiative forcing in the vicinity of Houston using a fully coupled meteorology-chemistry-aerosol model, J. Geophys. Res.-Atmos., 111, https://doi.org/10.1029/2005JD006721, 2006.

Gentry, B. M., Robinson, A. L., and Adams, P. J.: EASIUR-HR: A Model To Evaluate Exposure Inequality Caused by Ground-Level Sources of Primary Fine Particulate Matter, Environ. Sci. Technol., 57, 3817–3824, https://doi.org/10.1021/acs.est.2c06317, 2023.

Goodkind, A. L., Tessum, C. W., Coggins, J. S., Hill, J. D., and Marshall, J. D.: Fine-scale damage estimates of particulate matter air pollution reveal opportunities for location-specific mitigation of emissions, P. Natl. Acad. Sci. USA, 116, 8775–8780, https://doi.org/10.1073/pnas.1816102116, 2019.

Grell, G., Freitas, S. R., Stuefer, M., and Fast, J.: Inclusion of biomass burning in WRF-Chem: impact of wildfires on weather forecasts, Atmos. Chem. Phys., 11, 5289–5303, https://doi.org/10.5194/acp-11-5289-2011, 2011.

Grell, G. A. and Freitas, S. R.: A scale and aerosol aware stochastic convective parameterization for weather and air quality modeling, Atmos. Chem. Phys., 14, 5233–5250, https://doi.org/10.5194/acp-14-5233-2014, 2014.

Grell, G. A., Peckham, S. E., Schmitz, R., McKeen, S. A., Frost, G., Skamarock, W. C., and Eder, B.: Fully coupled "online" chemistry within the WRF model, Atmos. Environ., 39, 6957–6975, https://doi.org/10.1016/j.atmosenv.2005.04.027, 2005.

Guenther, A., Jiang, X., Heald, C., Sakulyanontvittaya, T., Duhl, T., Emmons, L., and Wang, X.: The Model of Emissions of Gases and Aerosols from Nature version 2.1 (MEGAN2.1): an extended and updated framework for modeling biogenic emissions, Geosci. Model Dev., 5, 1471–1492, https://doi.org/10.5194/gmd-5-1471-2012, 2012.

Heo, J., Adams, P. J., and Gao, H. O.: Public Health Costs of Primary $PM_{2.5}$ and Inorganic $PM_{2.5}$ Precursor Emissions in the United States, Environ. Sci. Techno., 50, 6061–6070, https://doi.org/10.1021/acs.est.5b06125, 2016a.

Heo, J., Adams, P. J., and Gao, H. O.: Reduced-form modeling of public health impacts of inorganic $PM_{2.5}$ and precursor emissions, Atmos. Environ., 137, 80–89, https://doi.org/10.1016/j.atmosenv.2016.04.026, 2016b.

Hong, S.-Y., Noh, Y., and Dudhia, J.: A new vertical diffusion package with an explicit treatment of entrainment processes, Mon. Weather Rev., 134, 2318–2341, https://doi.org/10.1175/MWR3199.1, 2006.

Khomenko, S., Pisoni, E., Thunis, P., Bessagnet, B., Cirach, M., Iungman, T., Barboza, E. P., Khreis, H., Mueller, N., Tonne, C., de Hoogh, K., Hoek, G., Chowdhury, S., Lelieveld, J., and Nieuwenhuijsen, M.: Spatial and sector-specific contributions of emissions to ambient air pollution and mortality in European cities: a health impact assessment, Lancet Publ. Health, 8, 93–106, https://doi.org/10.1016/S2468-2667(23)00106-8, 2023.

Lin, Y.-L., Farley, R. D., and Orville, H. D.: Bulk parameterization of the snow field in a cloud model, J. Clim. Appl. Meteorol., 22, 1065–1092, https://doi.org/10.1175/1520-0450(1983)022<1065:BPOTSF>2.0.CO;2, 1983.

Maronga, B., Banzhaf, S., Burmeister, C., Esch, T., Forkel, R., Fröhlich, D., Fuka, V., Gehrke, K. F., Geletič, J., Giersch, S., Gronemeier, T., Groß, G., Heldens, W., Hellsten, A., Hoffmann, F., Inagaki, A., Kadasch, E., Kanani-Sühring, F., Ketelsen, K., Khan, B. A., Knigge, C., Knoop, H., Krč, P., Kurppa, M., Maamari, H., Matzarakis, A., Mauder, M., Pallasch, M., Pavlik, D., Pfafferott, J., Resler, J., Rissmann, S., Russo, E., Salim, M., Schrempf, M., Schwenkel, J., Seckmeyer, G., Schubert, S., Sühring, M., von Tils, R., Vollmer, L., Ward, S., Witha, B., Wurps, H., Zeidler, J., and Raasch, S.: Overview of the PALM model system 6.0, Geosci. Model Dev., 13, 1335–1372, https://doi.org/10.5194/gmd-13-1335-2020, 2020.

McDuffie, E. E., Martin, R. V., Spadaro, J. V., Burnett, R., Smith, S. J., O'Rourke, P., Hammer, M. S., van Donkelaar, A., Bindle, L., Shah, V., Jaeglé, L., Luo, G., Yu, F., Adeniran, J. A., Lin, J., and Brauer, M.: Source sector and fuel contributions to ambient $PM_{2.5}$ and attributable mortality across multiple spatial scales, Nat. Commun., 12, https://doi.org/10.1038/s41467-021-23853-y, 2021.

Mendez-Espinosa, J. F., Belalcazar, L. C., and Morales-Betancourt, R.: Regional air quality impact of northern South America biomass burning emissions, Atmos. Environ., 203, 131–140, https://doi.org/10.1016/j.atmosenv.2019.01.042, 2019.

Menut, L., Cholakian, A., Pennel, R., Siour, G., Mailler, S., Valari, M., Lugon, L., and Meurdesoif, Y.: The CHIMERE chemistry-transport model v2023r1, Geosci. Model Dev., 17, 5431–5457, https://doi.org/10.5194/gmd-17-5431-2024, 2024.

Mlawer, E. J., Taubman, S. J., Brown, P. D., Iacono, M. J., and Clough, S. A.: Radiative transfer for inhomogeneous atmospheres: RRTM, a validated correlated-k model for the longwave, J. Geophys. Res.-Atmos., 102, 16663–16682, https://doi.org/10.1029/97JD00237, 1997.

Morales Betancourt, R., Rojas Neisa, D. R., Piracoca, A., and Espitia Cano, S.: InMAP-Bog – Input data and configuration files for InMAP, Zenodo [data set], https://doi.org/10.5281/zenodo.19654866, 2026.

Muller, N. Z. and Mendelsohn, R.: Efficient Pollution Regulation: Getting the Prices Right, Am. Econ. Rev., 99, 1714–1739, https://doi.org/10.1257/aer.99.5.1714, 2009.

NCEP: NCEP FNL Operational Model Global Tropospheric Analyses, continuing from July 1999, Research Data Archive at the National Center for Atmospheric Research, Computational and Information Systems Laboratory, https://doi.org/10.5065/D6M043C6, 2000.

Nedbor-Gross, R., Henderson, B. H., Davis, J. R., Pachón, J. E., Rincón, A., Guerrero, O. J., and Grajales, F.: Comparing Standard to Feature-Based Meteorological Model Evaluation Techniques in Bogotá, Colombia, J. Appl. Meteorol. Clim., 56, 391–413, https://doi.org/10.1175/JAMC-D-16-0058.1, 2017.

Orellano, P., Reynoso, J., Quaranta, N., Bardach, A., and Ciapponi, A.: Short-term exposure to particulate matter

(PM_{10} and $PM_{2.5}$), nitrogen dioxide (NO_2), and ozone (O_3) and all-cause and cause-specific mortality: Systematic review and meta-analysis, Environ. Int., 142, 105876, https://doi.org/10.1016/j.envint.2020.105876, 2020.

Pachón, J. E., Galvis, B., Lombana, O., Carmona, L. G., Fajardo, S., Rincón, A., Meneses, S., Chaparro, R., Nedbor-Gross, R., and Henderson, B.: Development and evaluation of a comprehensive atmospheric emission inventory for air quality modeling in the megacity of Bogotá, Atmosphere, 9, https://doi.org/10.3390/atmos9020049, 2018.

Pérez-Peña, M. P., Henderson, B. H., Nedbor-Gross, R., and Pachón, J. E.: Natural mitigation factor adjustment for re-suspended particulate matter emissions inventory for Bogotá, Colombia, Atmos. Pollut. Res., 8, 29–37, https://doi.org/10.1016/j.apr.2016.07.006, 2017.

Powers, J. G., Klemp, J. B., Skamarock, W. C., Davis, C. A., Dudhia, J., O, D. G., Coen, J. L., Gochis, D. J., Ahmadov, R., Peckham, S. E., Grell, G. A., Michalakes, J., Trahan, S., Benjamin, S. G., Alexander, C. R., Dimego, G. J., Wang, W., Schwartz, C. S., Romine, G. S., Liu, Z., Snyder, C., Chen, F., Barlage, M. J., Yu, W., and Michael, G.: The Weather Research and Forecasting Model: Overview, system efforts, and future directions, B. Am. Meteorol. Soc., 98, 1717–1737, https://doi.org/10.1175/BAMS-D-15-00308.1, 2017.

Resler, J., Krč, P., Belda, M., Juruš, P., Benešová, N., Lopata, J., Vlček, O., Damašková, D., Eben, K., Derbek, P., Maronga, B., and Kanani-Sühring, F.: PALM-USM v1.0: A new urban surface model integrated into the PALM large-eddy simulation model, Geosci. Model Dev., 10, 3635–3659, https://doi.org/10.5194/gmd-10-3635-2017, 2017.

Rincón-Riveros, J. M., Rincón-Caro, M. A., Sullivan, A. P., Mendez-Espinosa, J. F., Belalcazar, L. C., Quirama Aguilar, M., and Morales Betancourt, R.: Long-term brown carbon and smoke tracer observations in Bogotá, Colombia: association with medium-range transport of biomass burning plumes, Atmos. Chem. Phys., 20, 7459–7472, https://doi.org/10.5194/acp-20-7459-2020, 2020.

Rojas Neisa, D. R., Betancourt, M., and Espitia Cano, S.: WRF-Chem_v3.9.1 – Northern South America run for year 2018: Source code and configuration files, Zenodo [data set], https://doi.org/10.5281/zenodo.19655777, 2026.

Stockwell, W. R., Middleton, P., Chang, J. S., and Tang, X.: The second generation regional acid deposition model chemical mechanism for regional air quality modeling, J. Geophys. Res.-Atmos., 95, 16343–16367, https://doi.org/10.1029/JD095iD10p16343, 1990.

Stockwell, W. R., Kirchner, F., Kuhn, M., and Seefeld, S.: A new mechanism for regional atmospheric chemistry modeling, J. Geophys. Res.-Atmos., 102, 25847–25879, https://doi.org/10.1029/97JD00849, 1997.

Tessum, C. W., Hill, J. D., and Marshall, J. D.: Twelve-month, 12 km resolution North American WRF-Chem v3.4 air quality simulation: performance evaluation, Geosci. Model Dev., 8, 957–973, https://doi.org/10.5194/gmd-8-957-2015, 2015.

Tessum, C. W., Hill, J. D., and Marshall, J. D.: InMAP: A model for air pollution interventions, PLOS ONE, 12, 1–26, https://doi.org/10.1371/journal.pone.0176131, 2017.

Tessum, M. W., Anenberg, S. C., Chafe, Z. A., Henze, D. K., Kleiman, G., Kheirbek, I., Marshall, J. D., and Tessum, C. W.: Sources of ambient $PM_{2.5}$ exposure in 96 global cities, Atmos. Environ., 286, 119234, https://doi.org/10.1016/j.atmosenv.2022.119234, 2022.

Thakrar, S. K., Tessum, C. W., Apte, J. S., Balasubramanian, S., Millet, D. B., Pandis, S. N., Marshall, J. D., and Hill, J. D.: Global, high-resolution, reduced-complexity air quality modeling for PM2.5 using InMAP (Intervention Model for Air Pollution), PLOS ONE, 17, 1–22, https://doi.org/10.1371/journal.pone.0268714, 2022.

Thunis, P., Degraeuwe, B., Pisoni, E., Ferrari, F., and Clappier, A.: On the design and assessment of regional air quality plans: The SHERPA approach, J. Environ. Manage., 183, 952–958, https://doi.org/10.1016/j.jenvman.2016.09.049, 2016.

Thunis, P., Degraeuwe, B., Pisoni, E., Trombetti, M., Peduzzi, E., Belis, C., Wilson, J., Clappier, A., and Vignati, E.: $PM_{2.5}$ source allocation in European cities: A SHERPA modelling study, Atmos. Environ., 187, 93–106, https://doi.org/10.1016/j.atmosenv.2018.05.062, 2018.

Wheeler, S. M.: Built landscapes of metropolitan regions: An international typology, J. Am. Plan. Assoc., 81, 167–190, https://doi.org/10.1080/01944363.2015.1081567, 2015.

WHO: WHO global air quality guidelines. Particulate matter ($PM_{2.5}$ and PM_{10}), ozone, nitrogen dioxide, sulfur dioxide and carbon monoxide, https://www.who.int/publications/i/item/9789240034228 (last access: 16 November 2026), 2021.

Wiedinmyer, C., Akagi, S., Yokelson, R. J., Emmons, L., Al-Saadi, J., Orlando, J., and Soja, A.: The Fire INventory from NCAR (FINN): A high resolution global model to estimate the emissions from open burning, Geosci. Model Dev., 4, 625–641, https://doi.org/10.5194/gmd-4-625-2011, 2011.

Wu, R., Tessum, C. W., Zhang, Y., Hong, C., Zheng, Y., Qin, X., Liu, S., and Zhang, Q.: Reduced-complexity air quality intervention modeling over China: the development of InMAPv1.6.1-China and a comparison with CMAQv5.2, Geosci. Model Dev., 14, 7621–7638, https://doi.org/10.5194/gmd-14-7621-2021, 2021.